Contents

1 e-H V-Matrix **2**
1.1 Implementation . . . 2
1.1.1 Calculation of Direct Matrix Elements $D_{f,i}(k',k)$ . . . 2
1.1.2 Calculation of Exchange Matrix Elements $X_{f,i}(k',k)$ . . . 3
1.1.3 Evaluation of Integrals . . . 3
1.2 Direct Matrix Elements . . . 4
1.3 Exchange Matrix Elements . . . 6
1.3.1 $X_{f,i}(k',k)$ for $E = 10\,\mathrm{eV}$ . . . 6
1.3.2 $X_{f,i}(k',k)$ for $E = 1\,\mathrm{eV}$ . . . 8
1.4 On-Shell Matrix Elements . . . 10

2 V_{12} Potential in S-Wave Model **12**

3 Reduced CCC Code **14**
3.1 Triplet Half-on-Shell Matrix Elements . . . 14
3.2 Total Cross Sections . . . 14

List of Figures

1 Direct Matrix Elements 1s-1s . . . 4
2 Direct Matrix Elements 1s-2s . . . 5
3 Direct Matrix Elements 1s-3s . . . 5
4 Exchange Matrix Elements 1s-1s . . . 6
5 Exchange Matrix Elements 1s-2s . . . 7
6 Exchange Matrix Elements 1s-3s . . . 7
7 Exchange Matrix Elements 1s-1s . . . 8
8 Exchange Matrix Elements 1s-2s . . . 9
9 Exchange Matrix Elements 1s-3s . . . 9
10 On-Shell Matrix Elements 1s-1s . . . 10
11 On-Shell Matrix Elements 1s-2s . . . 11
12 On-Shell Matrix Elements 1s-3s . . . 11
13 Triplet $\theta = 0$ . . . 14
14 Triplet $\theta = 1$ . . . 15
15 Triplet $\theta = 2$ . . . 15
16 Total Cross Sections for $[1s \to 1s]$ . . . 16
17 Total Cross Sections for $[1s \to 2s]$ . . . 16
18 Total Cross Sections for $[1s \to 3s]$ . . . 17
19 Total Cross Sections for $[1s \to 4s]$ . . . 17
20 Total Cross Sections for $[1s \to 5s]$ . . . 18

List of Tables

The entire code repository used to calculate the data for this report can be found at https://github.com/dgsaf/acqm-workshop-5. Note that section 3 has not yet been attempted - it may be at a later date if time permits.

1 e-H V-Matrix

1.1 Implementation

We denote the hydrogen target states by $|\phi_i\rangle$, and we denote the electron projectile states by $|\mathbf{k}\rangle$ corresponding to continuum waves with energy $\frac{1}{2}k^2$, where $k = \|\mathbf{k}\|$. We shall work in the s-wave model; that is, we only consider target states with $\ell_i = 0$ and $m_i = 0$, and continuum states with

$$\langle \mathbf{r}|\mathbf{k}\rangle = N_k \sin(rk).$$

Note that we shall neglect the normalisation constants N_k henceforth. We calculate potential matrix elements of the form

$$\begin{aligned}
V^{(S)}_{f,i}(k', k) &= \langle k', \phi_f|\hat{V}^S|\phi_i, k\rangle \\
&= \langle k', \phi_f|\hat{V} - (-1)^S(E - \hat{H})\hat{P}_r|\phi_i, k\rangle \\
&= \langle k', \phi_f|\hat{V}_1 + \hat{V}_{1,2}|\phi_i, k\rangle - (-1)^S \langle k', \phi_f|E - \hat{H}|k, \phi_i\rangle \\
&= D_{f,i}(k', k) - (-1)^S X_{f,i}(k', k)
\end{aligned}$$

where $D_{f,i}(k', k)$ is the direct matrix element, $X_{f,i}(k', k)$ is the exchange matrix element, and where $\hat{V}_1$ is the electron-nuclear potential of the form

$$\hat{V}_1 = -\frac{1}{r_1},$$

and where $\hat{V}_{1,2}$ is the electron-electron potential of the form

$$\hat{V}_{1,2} = \frac{1}{\|\mathbf{r}_1 - \mathbf{r}_2\|} = \sum_{\lambda=0}^{\infty} \frac{4\pi}{2\lambda + 1} \frac{r_<^\lambda}{r_>^{\lambda+1}} \sum_{\mu=-\lambda}^{\lambda} Y^\mu_\lambda(\Omega_1) Y^{\mu *}_\lambda(\Omega_2)$$

where $r_< = \min(r_1, r_2)$, $r_> = \max(r_1, r_2)$, and where Y^μ_λ are the spherical harmonics. However, within the s-wave model this potential reduces to the form

$$\hat{V}_{1,2} = \frac{1}{r_>} = \frac{1}{\max(r_1, r_2)}.$$

1.1.1 Calculation of Direct Matrix Elements $D_{f,i}(k', k)$

The direct matrix elements are of the form

$$D_{f,i}(k', k) = \langle k', \phi_f|\hat{V}_1 + \hat{V}_{1,2}|\phi_i, k\rangle$$

where

$$\begin{aligned}
\langle k', \phi_f|\hat{V}_1|\phi_i, k\rangle &= \langle k'|\hat{V}_1|k\rangle \langle \phi_f|\phi_i\rangle \\
&= -\int_0^\infty \frac{1}{r_1} \sin(k'r_1)\sin(kr_1)\, \mathrm{d}r_1 \int_0^\infty \phi_f(r_2)\phi_i(r_2)\, \mathrm{d}r_2 \\
&= -\int_0^\infty \frac{1}{r_1} \sin(k'r_1)\sin(kr_1)\, \mathrm{d}r_1\, \delta_{f,i}
\end{aligned}$$

and where

$$\begin{aligned}
\langle k', \phi_f|\hat{V}_{1,2}|\phi_i, k\rangle &= \int_0^\infty \int_0^\infty \sin(k'r_1)\phi_f(r_2) \frac{1}{\max(r_1, r_2)} \sin(kr_1)\phi_i(r_2)\, \mathrm{d}r_1\, \mathrm{d}r_2 \\
&= \int_0^\infty \sin(k'r_1)\sin(kr_1) \left(\int_0^\infty \frac{1}{\max(r_1, r_2)} \phi_f(r_2)\phi_i(r_2)\, \mathrm{d}r_2 \right) \mathrm{d}r_1 \\
&= \int_0^\infty \sin(k'r_1)\sin(kr_1) \left(\frac{1}{r_1} \int_0^{r_1} \phi_f(r_2)\phi_i(r_2)\, \mathrm{d}r_2 + \int_{r_1}^\infty \frac{1}{r_2}\phi_f(r_2)\phi_i(r_2)\, \mathrm{d}r_2 \right) \mathrm{d}r_1 .
\end{aligned}$$

1.1.2 Calculation of Exchange Matrix Elements $X_{f,i}(k',k)$

The exchange matrix elements are of the form

$$\begin{aligned} X_{f,i}(k',k) =& \ \langle k',\phi_f|E-\hat{H}|k,\phi_i\rangle \\ =& \ (E-\tfrac{1}{2}k'^2-\tfrac{1}{2}k^2)\,\langle k'|\phi_i\rangle\,\langle\phi_f|k\rangle \\ & -\ \langle k'|\hat{V}_1|\phi_i\rangle\,\langle\phi_f|k\rangle - \langle k'|\phi_i\rangle\ \langle\phi_f|\hat{V}_2|k\rangle \\ & -\ \langle k',\phi_f|\hat{V}_{1,2}|k\phi_i\rangle \end{aligned}$$

where the one-electron inner products are of the form

$$\langle f|g\rangle = \int_0^\infty f(r)g(r)\,\mathrm{d}r$$

and where the two-electron inner product is of the form

$$\begin{aligned} \langle k',\phi_f|\hat{V}_{1,2}|k\phi_i\rangle \ =& \int_0^\infty\int_0^\infty \sin(k'r_1)\phi_f(r_2)\frac{1}{\max(r_1,r_2)}\phi_i(r_1)\sin(kr_2)\,\mathrm{d}r_1\,\mathrm{d}r_2 \\ =& \int_0^\infty \sin(k'r_1)\phi_i(r_1)\left(\int_0^\infty \frac{1}{\max(r_1,r_2)}\phi_f(r_2)\sin(kr_2)\,\mathrm{d}r_2\right)\mathrm{d}r_1 \\ =& \int_0^\infty \sin(k'r_1)\phi_i(r_1)\left(\frac{1}{r_1}\int_0^{r_1}\phi_f(r_2)\sin(kr_2)\,\mathrm{d}r_2+\int_{r_1}^\infty\frac{1}{r_2}\phi_f(r_2)\sin(kr_2)\,\mathrm{d}r_2\right)\mathrm{d}r_1 \end{aligned}$$

1.1.3 Evaluation of Integrals

We suppose that the radial functions are to be plotted on a radial grid of the form $\mathcal{R}=\{k\delta_r\}_{k=1}^{n_r}$ for $n_r>0$ and small $\delta_r>0$, and with a corresponding set of weights $\mathcal{W}=\{w_k\}_{k=1}^{n_r}$ such that

$$\int_0^\infty f(r)\,\mathrm{d}r = \lim_{n_r\to\infty}\sum_{k=1}^{n_r} w_k f(r_k) = \lim_{n_r\to\infty}\sum_{k=1}^{n_r} w_k f_k \approx \sum_{k=1}^{n_r} w_k f_k.$$

The one-electron integrals, of the form $\langle f|g\rangle$, are then evaluated in the following manner

$$\langle f|g\rangle = \int_0^\infty f(r)g(r)\,\mathrm{d}r \approx \sum_{k=1}^{n_r} w_k f_k g_k.$$

The two electron integrals $\langle F|\,|G\rangle$ where

$$\langle F|\,|G\rangle = \int_0^\infty F(r_1)\left(\frac{1}{r_1}\int_0^{r_1} G(r_2)\,\mathrm{d}r_2 + \int_{r_1}^\infty \frac{1}{r_2}G(r_2)\,\mathrm{d}r_2\right)\mathrm{d}r_1\,,$$

are evaluated in the following manner

$$\langle F|\,|G\rangle \approx \sum_{k=1}^{n_r} w_k F_k\left(\frac{1}{r_k}A_k + B_k\right)$$

where

$$A_k = \sum_{m=1}^{k} w_m G_m = \begin{cases} A_{k-1}+w_kG_k & \text{for} \quad k=2,\ldots,n_r \\ w_kG_k & \text{for} \quad k=1 \end{cases}$$

and

$$B_k = \sum_{m=k}^{n_r}\frac{1}{r_m}w_mG_m = \begin{cases} B_{k+1}+\frac{1}{r_k}w_kG_k & \text{for} \quad k=1,\ldots,n_r-1 \\ \frac{1}{r_k}w_kG_k & \text{for} \quad k=n_r \end{cases}.$$

For these calculations, we have used: a radial grid of the form $\mathcal{R} = \{i\delta_r\}_{i=1}^{n_r}$, with $\delta_r = 0.01$ and $\max(\mathcal{R}) = 100$, and a momentum grid of the form $\mathcal{K} = \{i\delta_k\}_{i=1}^{n_k}$, with $\delta_k = 0.025$ and $\max(\mathcal{K}) = 5$.

1.2 Direct Matrix Elements

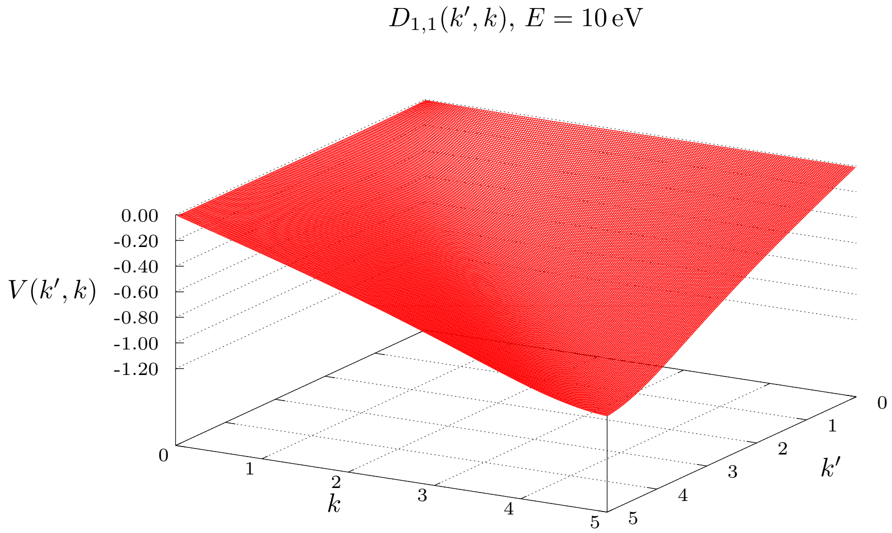

Figure 1: The $D_{f,i}(k', k)$ direct matrix elements (shown in red) are presented for the $1s \to 1s$ transition, with $E = 10\,\mathrm{eV}$.

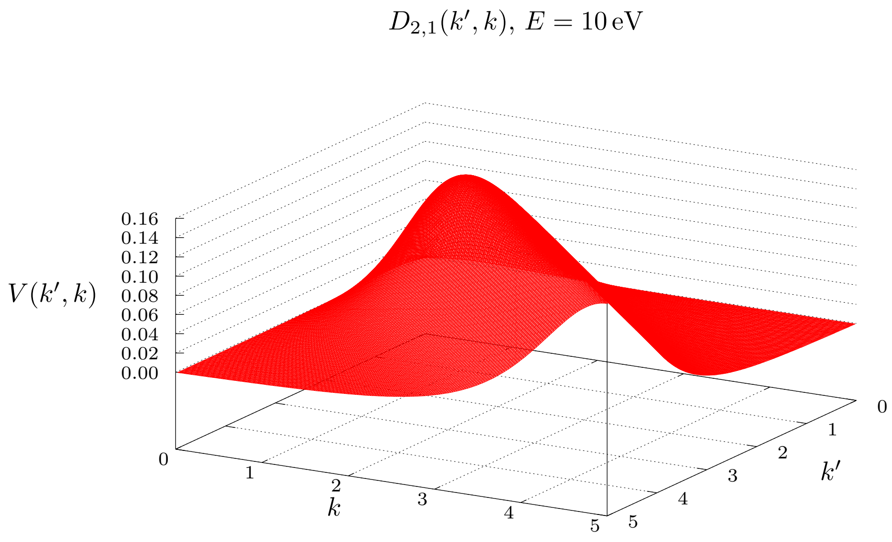

Figure 2: The $D_{f,i}(k', k)$ direct matrix elements (shown in red) are presented for the $1s \rightarrow 2s$ transition, with $E = 10\,\mathrm{eV}$.

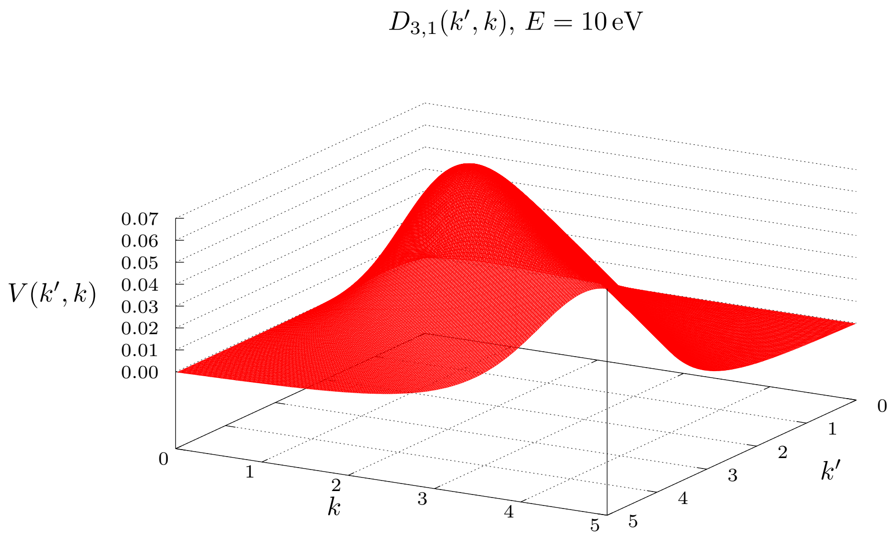

Figure 3: The $D_{f,i}(k', k)$ direct matrix elements (shown in red) are presented for the $1s \rightarrow 3s$ transition, with $E = 10\,\mathrm{eV}$.

1.3 Exchange Matrix Elements

1.3.1 $X_{f,i}(k', k)$ for $E = 10\,\mathrm{eV}$

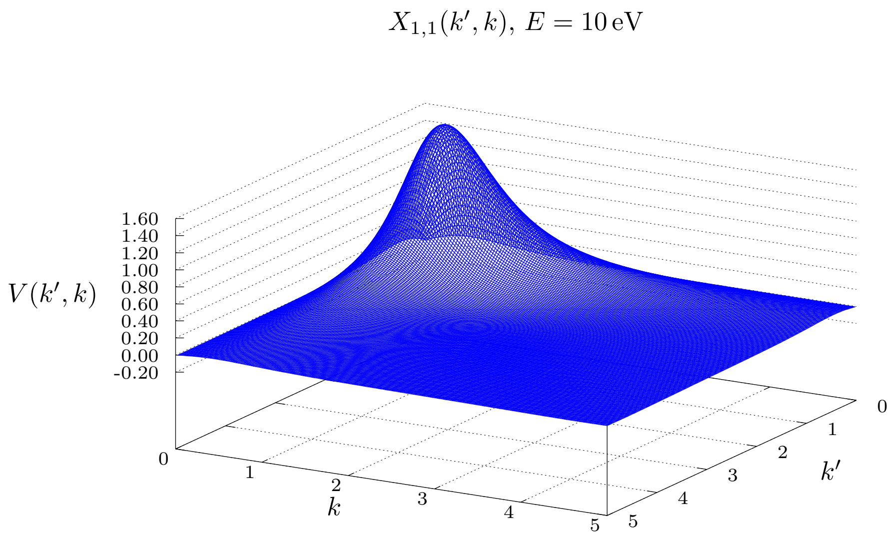

Figure 4: The $X_{f,i}(k', k)$ exchange matrix elements (shown in blue) are presented for the $1s \to 1s$ transition, with $E = 10\,\mathrm{eV}$.

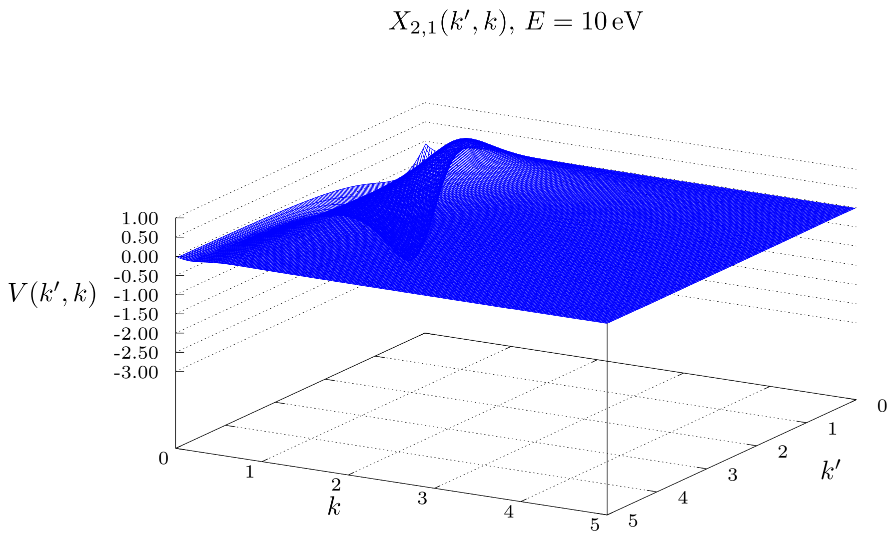

Figure 5: The $X_{f,i}(k', k)$ exchange matrix elements (shown in blue) are presented for the $1s \to 2s$ transition, with $E = 10\,\mathrm{eV}$.

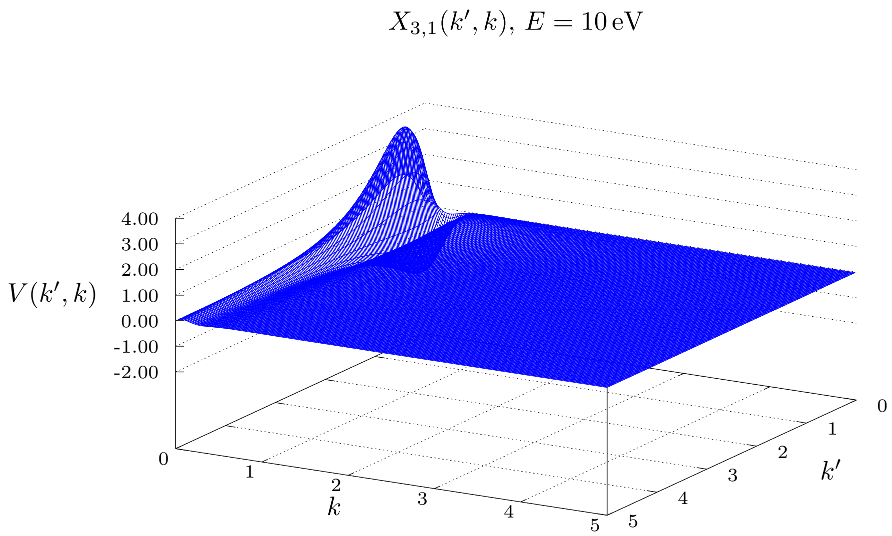

Figure 6: The $X_{f,i}(k', k)$ exchange matrix elements (shown in blue) are presented for the $1s \to 3s$ transition, with $E = 10\,\mathrm{eV}$.

1.3.2 $X_{f,i}(k', k)$ for $E = 1\,\mathrm{eV}$

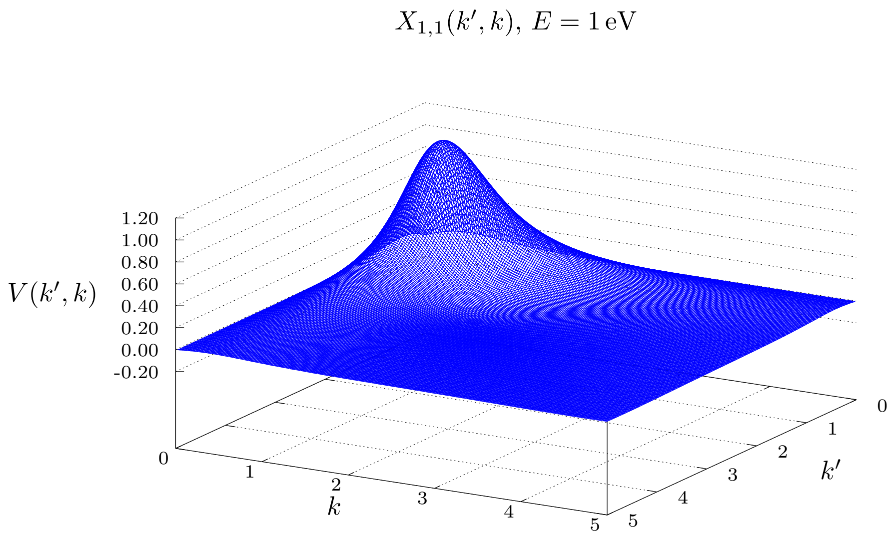

Figure 7: The $X_{f,i}(k', k)$ exchange matrix elements (shown in blue) are presented for the $1s \to 1s$ transition, with $E = 1\,\mathrm{eV}$.

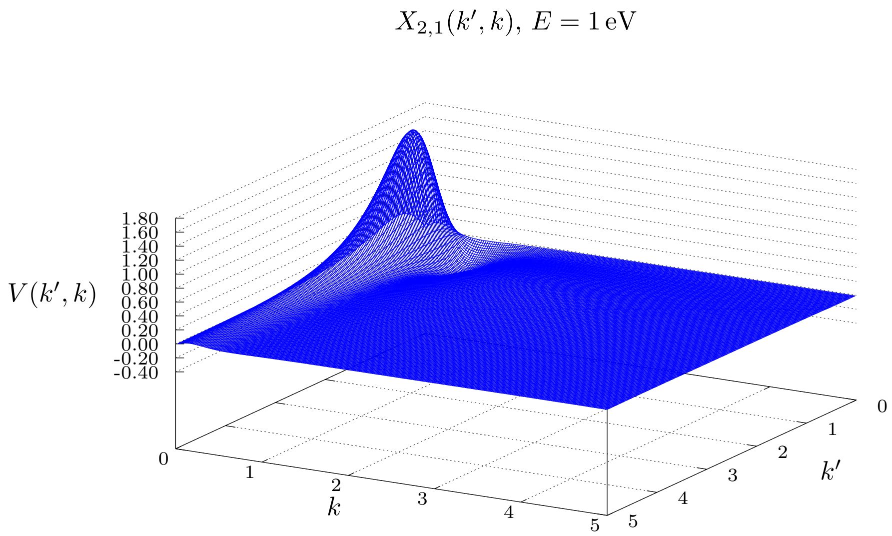

Figure 8: The $X_{f,i}(k', k)$ exchange matrix elements (shown in blue) are presented for the $1s \to 2s$ transition, with $E = 1\,\mathrm{eV}$.

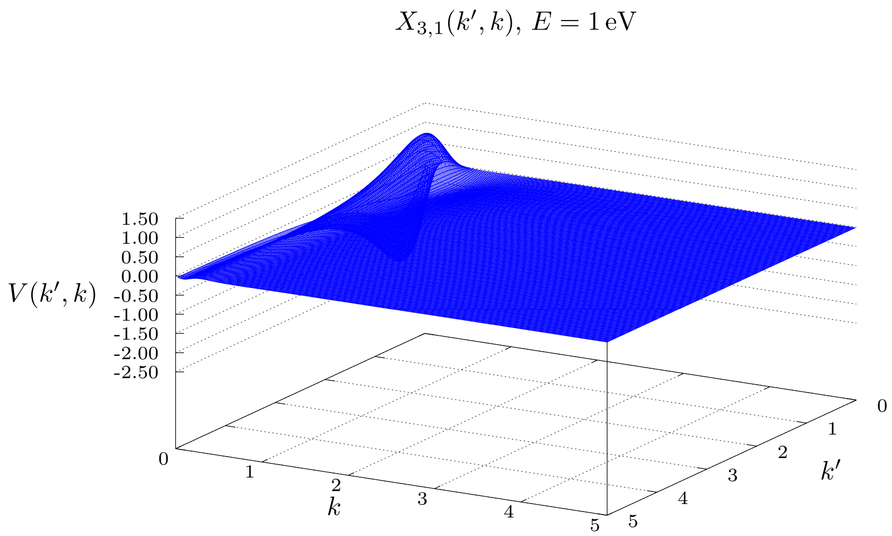

Figure 9: The $X_{f,i}(k', k)$ exchange matrix elements (shown in blue) are presented for the $1s \to 3s$ transition, with $E = 1\,\mathrm{eV}$.

1.4 On-Shell Matrix Elements

For the transisiton $[i \to f]$, the on-shell energy is of the form

$$\epsilon_i + \frac{1}{2}k^2 = E = \epsilon_f + \frac{1}{2}k'^2$$

whence the on-shell value for k' is defined by

$$\frac{1}{2}k'^2 = E - \epsilon_f = \frac{1}{2}k^2 + \epsilon_i - \epsilon_f$$

where for the case of a hydrogen target, with $\epsilon_n = -\frac{1}{2n^2}$, and $i = 1$, we have have that

$$k' = \sqrt{k^2 - \frac{f^2 - 1}{f^2}}.$$

Note that transitions are forbidden for

$$k^2 < \frac{f^2 - 1}{f^2} = 1 - \frac{1}{f^2}.$$

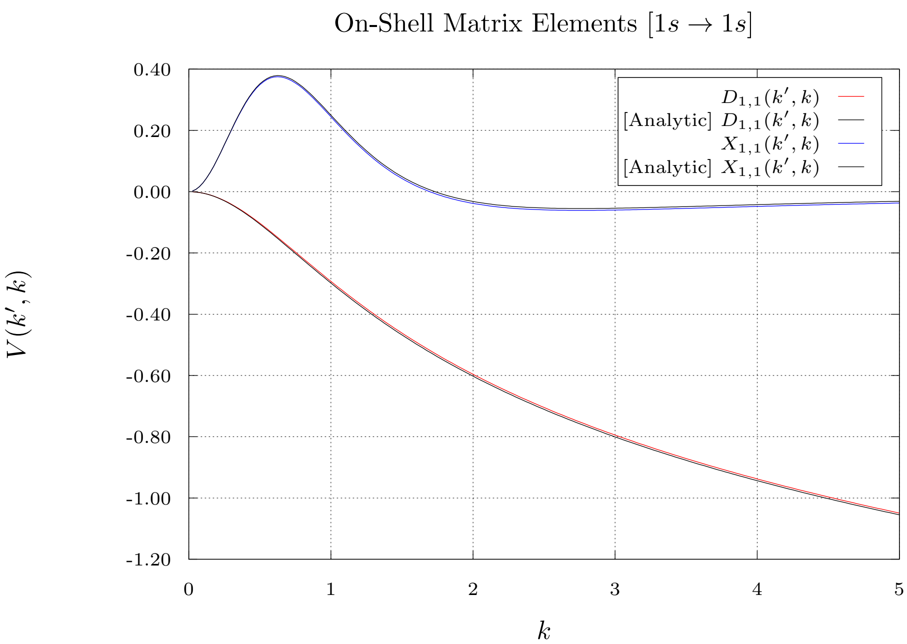

Figure 10: The $D_{f,i}(k', k)$ direct and $X_{f,i}(k', k)$ exchange on-shell matrix elements (shown in red and blue respectively) are presented for the $1s \to 1s$ transition, and are compared with their respective analytic expressions (shown in black).

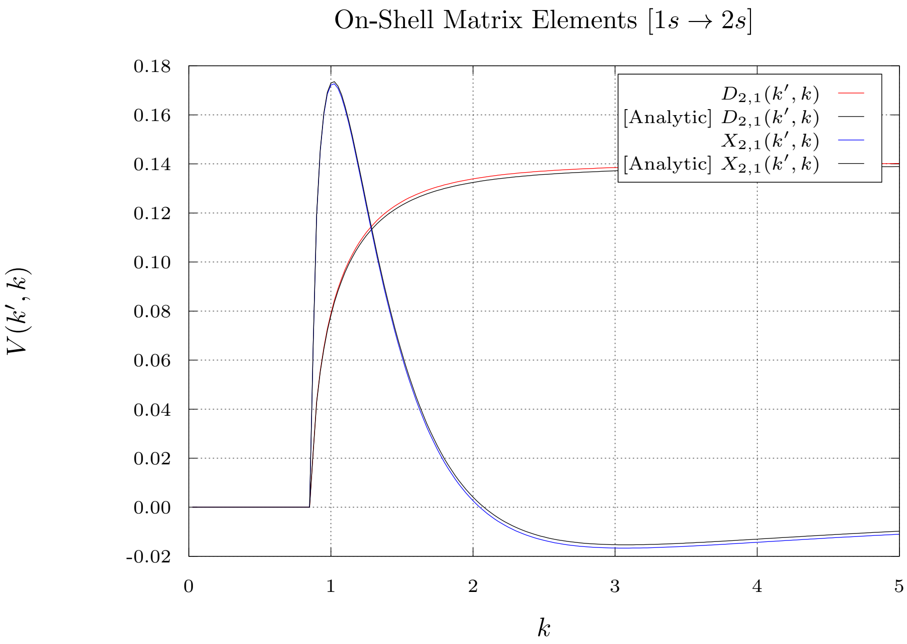

Figure 11: The $D_{f,i}(k', k)$ direct and $X_{f,i}(k', k)$ exchange on-shell matrix elements (shown in red and blue respectively) are presented for the $1s \to 2s$ transition, and are compared with their respective analytic expressions (shown in black).

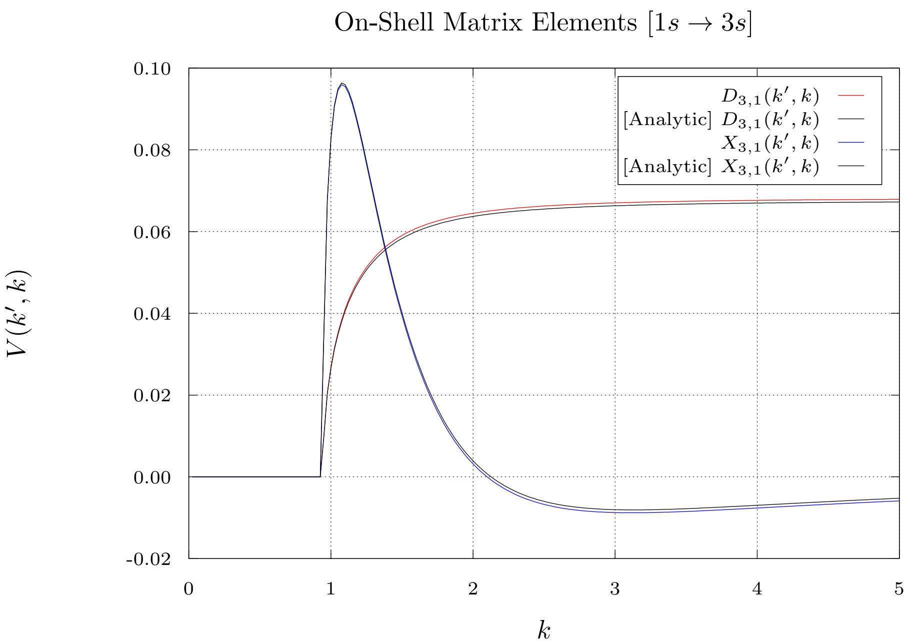

Figure 12: The $D_{f,i}(k', k)$ direct and $X_{f,i}(k', k)$ exchange on-shell matrix elements (shown in red and blue respectively) are presented for the $1s \to 3s$ transition, and are compared with their respective analytic expressions (shown in black).

2 V_{12} Potential in S-Wave Model

We note that the general form for a continuum wave $|\mathbf{k}\rangle = |k, \ell, m\rangle$ is

$$\langle \mathbf{r}|\mathbf{k}\rangle = \frac{1}{r} u_\ell(r;k) Y_\ell^m(\Omega),$$

and that the general form for the hydrogen target states $|\phi_i\rangle = |\phi_{n_i,\ell_i,m_i}\rangle$ is

$$\langle \mathbf{r}|\phi_i\rangle = \frac{1}{r}\phi_i(r) Y_{\ell_i}^{m_i}(\Omega).$$

Recall that the electron-electron potential is of the form

$$\hat{V}_{1,2} = \frac{1}{\|\mathbf{r}_1 - \mathbf{r}_2\|} = \sum_{\lambda=0}^{\infty} \frac{4\pi}{2\lambda+1} \frac{r_<^\lambda}{r_>^{\lambda+1}} \sum_{\mu=-\lambda}^{\lambda} Y_\lambda^\mu(\Omega_1) Y_\lambda^{\mu *}(\Omega_2)$$

where $r_< = \min(r_1, r_2)$, $r_> = \max(r_1, r_2)$, and where Y_λ^μ are the spherical harmonics. We now consider the form of the two-electron term in $D_{f,i}(\mathbf{k}', \mathbf{k})$,

$$\langle \mathbf{k}', \phi_f|\hat{V}_{1,2}|\phi_i, \mathbf{k}\rangle = \int\int \langle \mathbf{r}_1|\mathbf{k}'\rangle^* \langle \mathbf{r}_2|\phi_f\rangle^* \frac{1}{\|\mathbf{r}_1 - \mathbf{r}_2\|} \langle \mathbf{r}_1|\mathbf{k}\rangle \langle \mathbf{r}_2|\phi_i\rangle \, \mathrm{d}\mathbf{r}_1 \, \mathrm{d}\mathbf{r}_2$$

for which the partial wave expansion is of the form

$$\begin{aligned}
\langle \mathbf{k}', \phi_f|\hat{V}_{1,2}|\phi_i, \mathbf{k}\rangle &= \sum_{\lambda=0}^{\infty} \frac{4\pi}{2\lambda+1} \sum_{\mu=-\lambda}^{\lambda} \int_0^\infty \int_0^\infty \frac{u_{\ell'}(r_1;k')}{r_1} \frac{\phi_f(r_2)}{r_2} \frac{r_<^\lambda}{r_>^{\lambda+1}} \frac{\phi_i(r_2)}{r_2} \frac{u_\ell(r_1;k)}{r_1} r_1^2 r_2^2 \, \mathrm{d}r_1 \, \mathrm{d}r_2 \\
&\qquad \times \int_{S^2} Y_{\ell'}^{m'^*}(\Omega_1) Y_\lambda^\mu(\Omega_1) Y_\ell^m(\Omega_1) \, \mathrm{d}\Omega_1 \\
&\qquad \times \int_{S^2} Y_{\ell_f}^{m_f *}(\Omega_2) Y_\lambda^{\mu *}(\Omega_2) Y_{\ell_i}^{m_i}(\Omega_2) \, \mathrm{d}\Omega_2 \\
&= \sum_{\lambda=0}^{\infty} \frac{4\pi}{2\lambda+1} \sum_{\mu=-\lambda}^{\lambda} \int_0^\infty \int_0^\infty u_{\ell'}(r_1;k') \phi_f(r_2) \frac{r_<^\lambda}{r_>^{\lambda+1}} \phi_i(r_2) u_\ell(r_1;k) \, \mathrm{d}r_1 \, \mathrm{d}r_2 \\
&\qquad \times \int_{S^2} Y_{\ell'}^{m'^*}(\Omega_1) Y_\lambda^\mu(\Omega_1) Y_\ell^m(\Omega_1) \, \mathrm{d}\Omega_1 \\
&\qquad \times \int_{S^2} Y_{\ell_f}^{m_f *}(\Omega_2) Y_\lambda^{\mu *}(\Omega_2) Y_{\ell_i}^{m_i}(\Omega_2) \, \mathrm{d}\Omega_2 \,.
\end{aligned}$$

However, in the s-wave model, we have that that all ℓ, m terms (for the continuum wave) are zero, where therefore all $Y_\ell^m(\Omega) = Y_0^0(\Omega) = \frac{1}{\sqrt{4\pi}}$. It then follows that

$$\int_{S^2} Y_{\ell'}^{m'^*}(\Omega_1) Y_\lambda^\mu(\Omega_1) Y_\ell^m(\Omega_1) \, \mathrm{d}\Omega_1 = \frac{1}{\sqrt{4\pi}} \int_{S^2} Y_{\ell'}^{m'^*}(\Omega_1) Y_\lambda^\mu(\Omega_1) \, \mathrm{d}\Omega_1 = \frac{1}{\sqrt{4\pi}} \delta_{\ell',\lambda} \delta_{m',\mu}$$

and as $\ell', m' = 0$, the only non-zero term in the sum is where $\lambda = \mu = 0$. Whence, we have that

$$\begin{aligned}
\langle \mathbf{k}', \phi_f|\hat{V}_{1,2}|\phi_i, \mathbf{k}\rangle = \sqrt{4\pi} &\int_0^\infty \int_0^\infty u_{\ell'}(r_1;k') \phi_f(r_2) \frac{r_<^0}{r_>^1} \phi_i(r_2) u_\ell(r_1;k) \, \mathrm{d}r_1 \, \mathrm{d}r_2 \\
&\times \int_{S^2} Y_{\ell_f}^{m_f *}(\Omega_2) Y_0^{0*}(\Omega_2) Y_{\ell_i}^{m_i}(\Omega_2) \, \mathrm{d}\Omega_2 \\
= \quad &\int_0^\infty \int_0^\infty u_{\ell'}(r_1;k') \phi_f(r_2) \frac{1}{r_>} \phi_i(r_2) u_\ell(r_1;k) \, \mathrm{d}r_1 \, \mathrm{d}r_2 \\
&\times \int_{S^2} Y_{\ell_f}^{m_f *}(\Omega_2) Y_{\ell_i}^{m_i}(\Omega_2) \, \mathrm{d}\Omega_2 \\
= \quad &\int_0^\infty \int_0^\infty u_{\ell'}(r_1;k') \phi_f(r_2) \frac{1}{r_>} \phi_i(r_2) u_\ell(r_1;k) \, \mathrm{d}r_1 \, \mathrm{d}r_2 \\
&\times \delta_{\ell_f,\ell_i} \delta_{m_f,m_i}
\end{aligned}$$

and so we may restrict our attention to the case where $\ell_f = \ell_i$ and $m_f = m_i$; that is, where the angular momentum of the target is left unchanged. Finally, we have that

$$\langle \mathbf{k}', \phi_f | \hat{V}_{1,2} | \phi_i, \mathbf{k} \rangle = \langle k', \phi_f | \hat{V}_{1,2} | \phi_i, k \rangle = \int_0^\infty \int_0^\infty u_{\ell'}(r_1; k') \phi_f(r_2) \frac{1}{r_>} \phi_i(r_2) u_\ell(r_1; k) \, \mathrm{d}r_1 \, \mathrm{d}r_2$$

yielding the result as required.

3 Reduced CCC Code

3.1 Triplet Half-on-Shell Matrix Elements

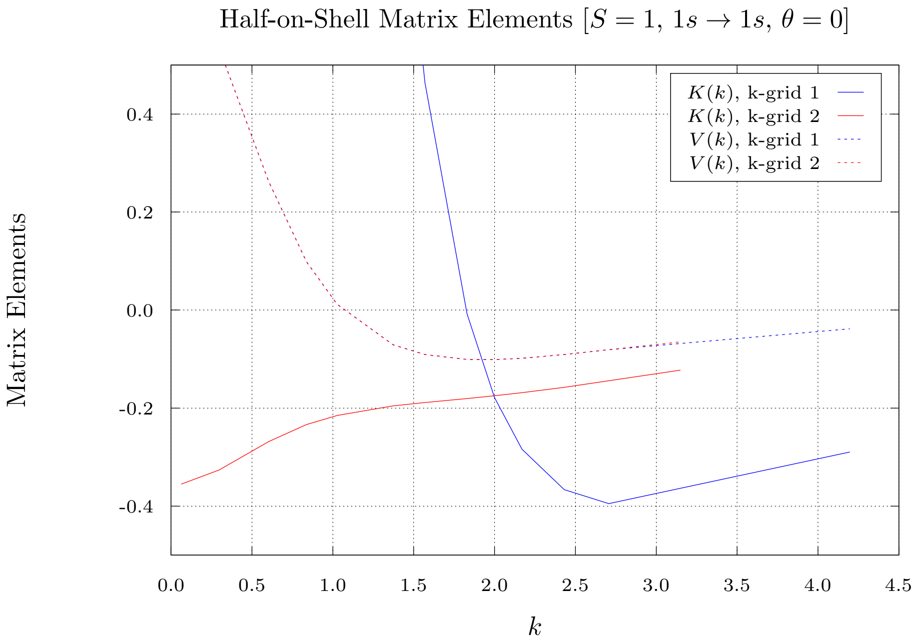

Figure 13: The triplet half-on-shell direct matrix elements, $K(k)$ (shown in solid lines) and $V(k)$ (shown in dashed lines), are presented for the $1s \to 1s$ transition, with $\theta = 0$, for both k-grids (shown in blue and red). Note that the $V(k)$ matrix elements overlap for both grids, on their common domain.

3.2 Total Cross Sections

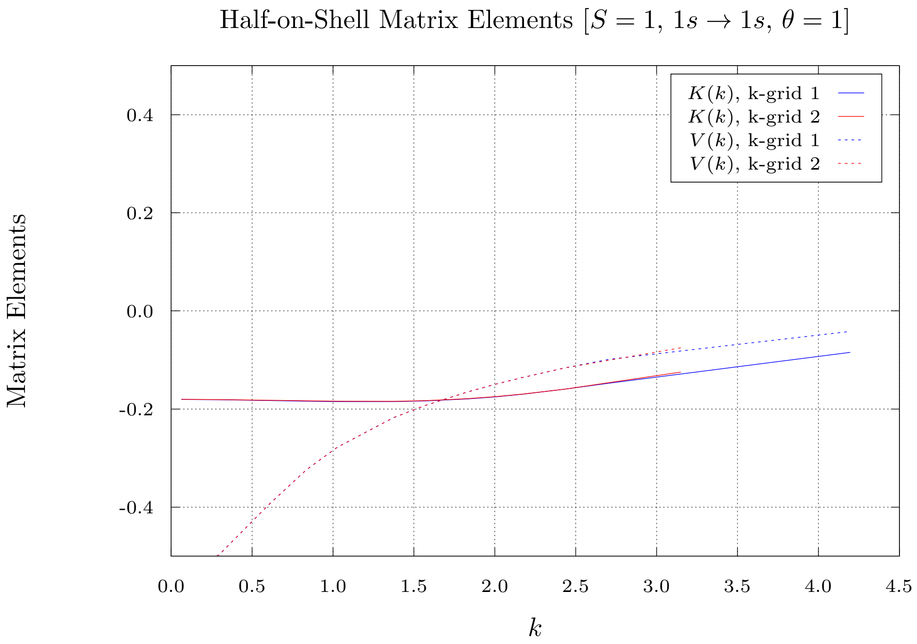

Figure 14: The triplet half-on-shell direct matrix elements, $K(k)$ (shown in solid lines) and $V(k)$ (shown in dashed lines), are presented for the $1s \to 1s$ transition, with $\theta = 1$, for both k-grids (shown in blue and red). Note that the $K(k)$ and $V(k)$ matrix elements overlap for both grids, on their common domain.

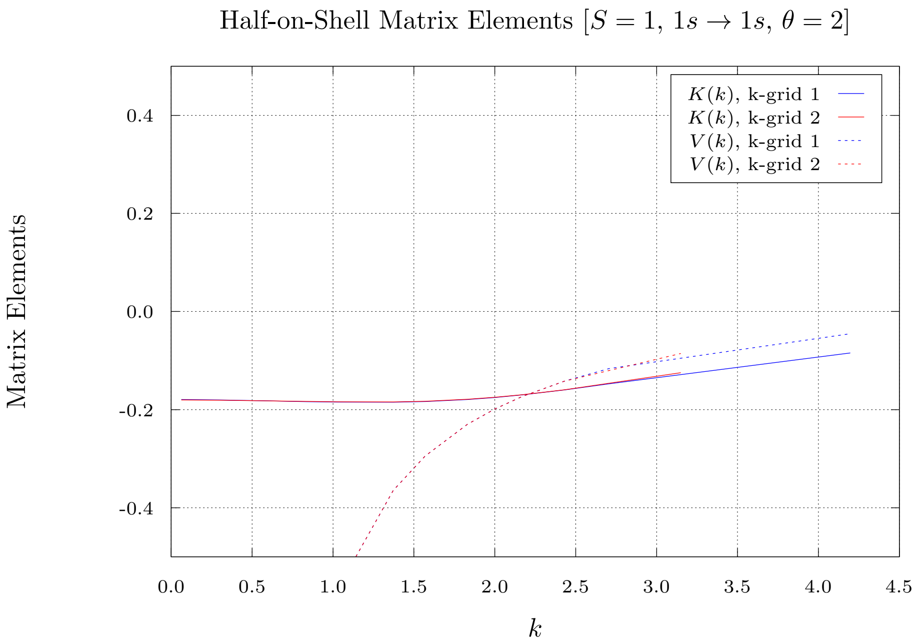

Figure 15: The triplet half-on-shell direct matrix elements, $K(k)$ (shown in solid lines) and $V(k)$ (shown in dashed lines), are presented for the $1s \to 1s$ transition, with $\theta = 2$, for both k-grids (shown in blue and red). Note that the $K(k)$ and $V(k)$ matrix elements overlap for both grids, on their common domain. Note also that the $K(k)$ matrix elements are essentially equivalent to those for $\theta = 1$, presented in Figure 14, even though the $V(k)$ matrix elements are different.

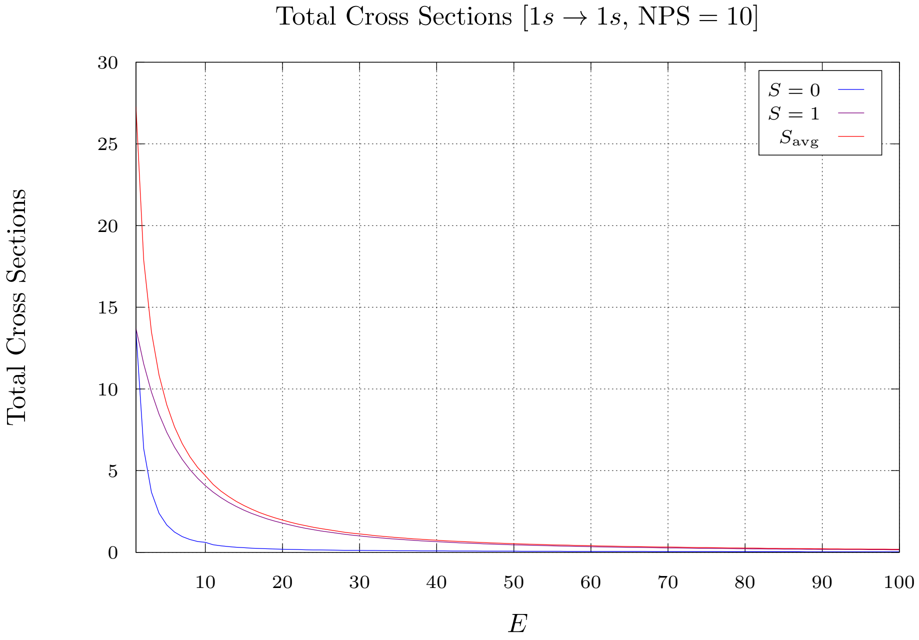

Figure 16: The total cross sections, for $S = 0$ (shown in blue), $S = 1$ (shown in purple), and S averaged (shown in red), are presented for the $[1s \to 1s]$ transition, from $1\,\mathrm{eV}$ to $100\,\mathrm{eV}$. Note that this calculation was performed with NPS = 10.

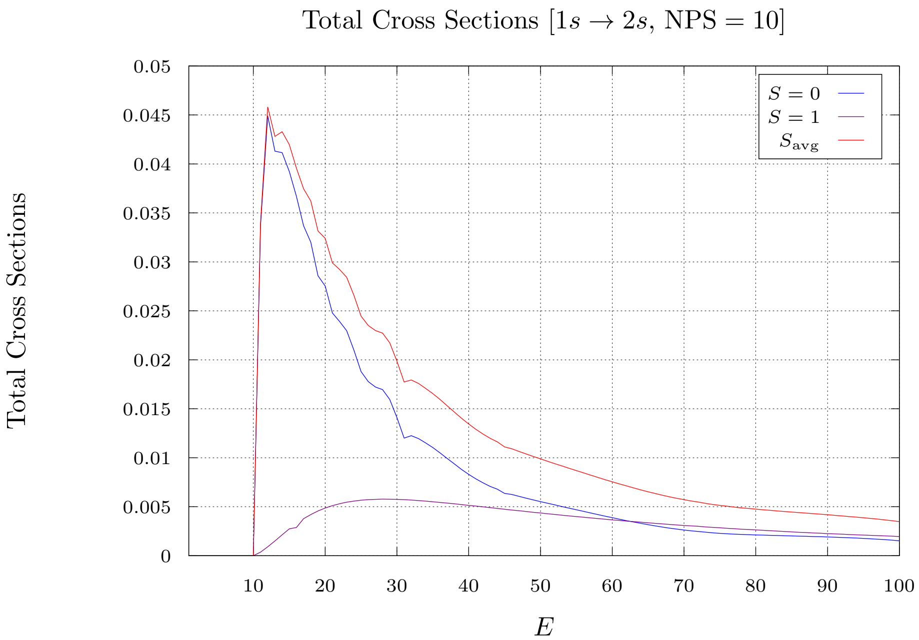

Figure 17: The total cross sections, for $S = 0$ (shown in blue), $S = 1$ (shown in purple), and S averaged (shown in red), are presented for the $[1s \to 2s]$ transition, from $1\,\mathrm{eV}$ to $100\,\mathrm{eV}$. Note that this calculation was performed with NPS = 10.

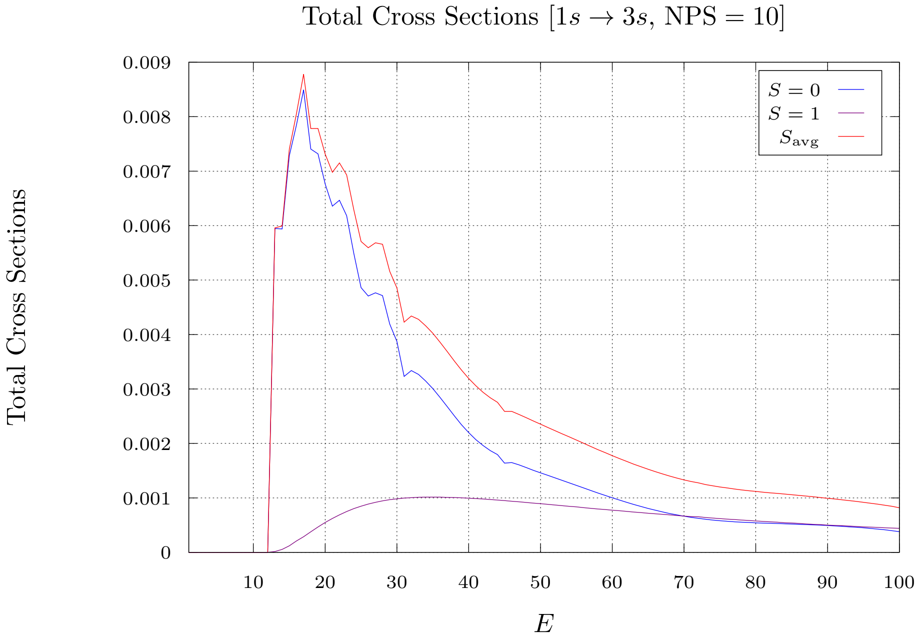

Figure 18: The total cross sections, for $S = 0$ (shown in blue), $S = 1$ (shown in purple), and S averaged (shown in red), are presented for the $[1s \rightarrow 3s]$ transition, from 1 eV *to* 100 eV*. Note that this calculation was performed with* NPS = 10.

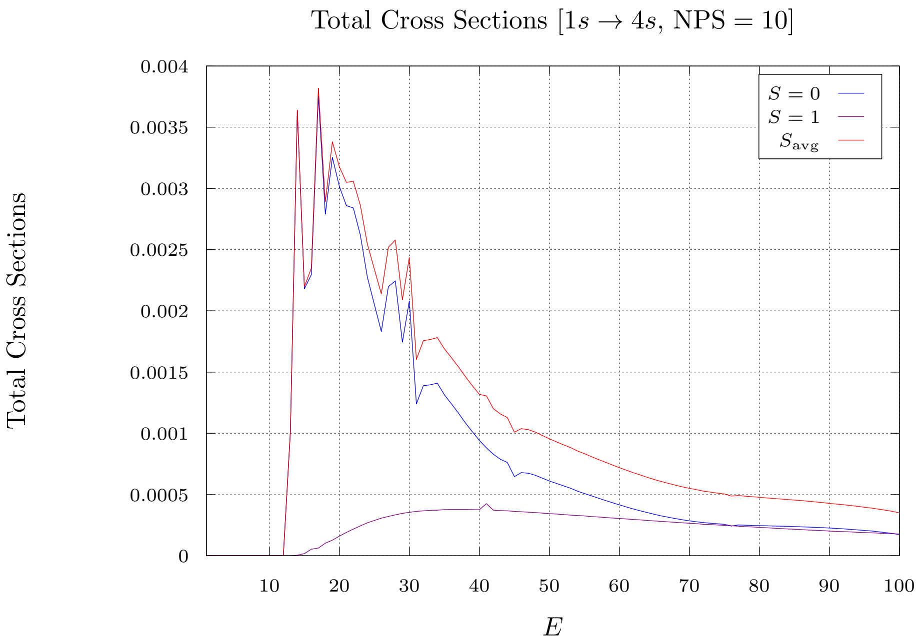

Figure 19: The total cross sections, for $S = 0$ (shown in blue), $S = 1$ (shown in purple), and S averaged (shown in red), are presented for the $[1s \rightarrow 4s]$ transition, from 1 eV *to* 100 eV*. Note that this calculation was performed with* NPS = 10.

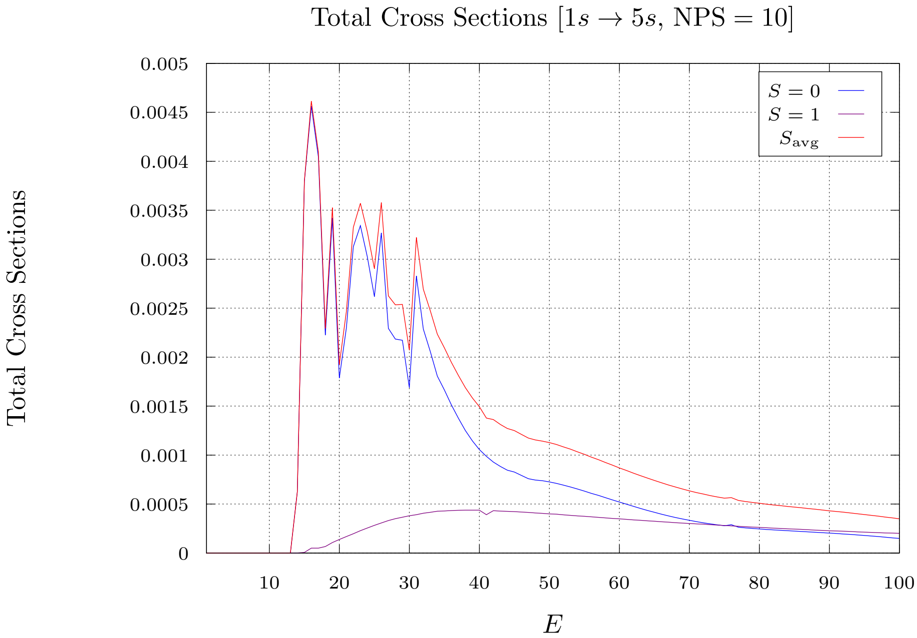

Figure 20: The total cross sections, for $S = 0$ (shown in blue), $S = 1$ (shown in purple), and S averaged (shown in red), are presented for the $[1s \to 5s]$ transition, from $1\,\mathrm{eV}$ to $100\,\mathrm{eV}$. Note that this calculation was performed with $\mathrm{NPS} = 10$.